Wang et al. *Zool. Res.* 2026, 47(4): 1166−1178
https://doi.org/10.24272/j.issn.2095-8137.2025.356
https://cstr.cn/32248.14.zr.2025.356

ZR | Zoological Research

Article Open Access

Unraveling the role of *Djstat5* in planarian regeneration by modulating cell proliferation and apoptosis

Du Wang[1,#], Han-Xue Zheng[1,#], Jia-Yi Chen[1], Meng-Di Cheng[1], Lin-Feng Li[1], Yu-Jie Nie[1], Yan-Mei Qiang[1], Wen-Juan Xue[1], Ruo-Han Lin[1], Xin Leng[1], Fu-Lin Chen[1,2,3,*], Yuan Yu[1,2,3,*]

[1] *Laboratory of Tissue Engineering*, *College of Life Sciences*, *Northwest University*, *Xi'an*, *Shaanxi* 710069, *China*

[2] *Provincial Key Laboratory of Biotechnology of Shaanxi*, *Northwest University*, *Xi'an*, *Shaanxi* 710069, *China*

[3] *Key Laboratory of Resource Biology and Biotechnology in Western China*, *Ministry of Education*, *College of Life Sciences*, *Northwest University*, *Xi'an*, *Shaanxi* 710069, *China*

ABSTRACT

Signal transducer and activator of transcription (STAT) proteins function as key mediators of cytokine signaling and are critically involved in stem cell regulation, tissue regeneration, and immune responses in vertebrates. However, their roles in invertebrate regeneration, particularly in adult pluripotent stem cell systems like those of planarians, remain largely unexplored. In this study, we investigated the function of *Djstat5*, a STAT5 homolog in the planarian *Dugesia japonica*, and demonstrated that it is dynamically upregulated during the early regenerative phases. RNA interference (RNAi)-mediated knockdown of *Djstat5* resulted in severe defects in tissue regeneration, including blastema hypoplasia, reduced mitotic activity, and diminished apoptosis. Transcriptomic analysis revealed that *Djstat5* knockdown led to upregulation of *Djnlrc3*, a putative negative regulator of regeneration. Functional interaction between *Djstat5* and *Djnlrc3* was further supported by double RNAi experiments, which showed that co-knockdown of *Djnlrc3* significantly rescued the regeneration defects induced by *Djstat5* loss. Together, our findings establish *Djstat5* as an essential regulator of planarian regeneration and provide new insights into conserved STAT-mediated signaling pathways in adult stem cell-based tissue regeneration.

Keywords: STAT5; Planarian; Regeneration; Stem cells

INTRODUCTION

Regeneration is one of the most remarkable biological phenomena, exemplified by the ability of certain animals—such as planarians (Chen & Lei, 2023; Reddien, 2018), salamanders (Bassat & Tanaka, 2021; Pan et al., 2023), and zebrafish (Han et al., 2019b; Jia et al., 2025; Shen et al., 2025)—to efficiently restore lost or damaged tissues. Studying these organisms has uncovered complex biological processes, including stem cell differentiation (Zheng et al., 2025), restoration of tissue polarity (Sun et al., 2025), and seamless integration of regenerated tissues (Doddihal et al., 2024), thereby advancing our understanding of regenerative mechanisms.

Among these models, planarians display extraordinary regenerative plasticity, driven by a population of adult pluripotent stem cells known as neoblasts (Ge et al., 2022). Following injury, neoblasts migrate to the wound site, proliferate, differentiate, and form blastemas that regenerate missing structures (Park et al., 2023; Reddien, 2021). This process involves two distinct mitotic waves: an initial systemic proliferation phase (4–10 h post-amputation, hpa), followed by a localized proliferative response at the wound site (48–72 hpa), which is coupled with neoblast differentiation (Wenemoser & Reddien, 2010). Notably, injury-induced apoptosis functions as a potential catalyst for regeneration, by generating a signaling microenvironment that actively promotes cell renewal and proliferation (Adell et al., 2025; Chera et al., 2009; Pellettieri et al., 2010). This finding suggests a model in which the balance between cell production and elimination is dynamically coordinated to ensure proper regeneration. Several genes, such as *fir1* (Han et al., 2019a) and *pi3k* (Zheng et al., 2021), have been shown to help coordinate this balance between apoptosis and neoblast proliferation. However, the molecular mechanisms that translate early injury signals into the activation of neoblast proliferation remain incompletely understood.

Received: 22 November 2025; Accepted: 09 December 2025; Online: 07 January 2026

Foundation items: This work was supported by the National Natural Science Foundation of China (31900330), the Natural Science Basic Research Plan in Shaanxi Province of China (2024JC-YBMS-182, 2025JC-YBMS-1013 and 2024JC-YBMS-135), the Shaanxi Fundamental Science Research Project for Chemistry and Biology (23JHQ067), and the Postdoctoral Fellowship Program of the China Postdoctoral Science Foundation (GZC20232148).

[#]Authors contributed equally to this work

*Corresponding authors, E-mail: chenfl@nwu.edu.cn; yuyuan@nwu.edu.cn

STAT5, a core member of the signal transducer and activator of transcription (STAT) transcription factor family, functions as a pivotal intracellular signaling hub that transduces extracellular cues, such as cytokines and growth factors, into transcriptional responses governing fundamental cellular processes (Hu et al., 2021; Xue et al., 2023). The activation of this pathway involves a series of events, including receptor activation, tyrosine phosphorylation, nuclear translocation, and transcriptional regulation of target genes, which collectively modulate diverse biological processes such as tissue repair, cell proliferation, and apoptosis (Awasthi et al., 2021; Dai et al., 2025; Li & Huang, 2024; Lin et al., 2024; Lv et al., 2024; Mustafa et al., 2024). In mammals such as *Mus musculus* (mouse) and *Homo sapiens* (human), STAT5, which comprises two isoforms (STAT5A and STAT5B), has been extensively studied as a key regulator of genes involved in cell survival, metabolic homeostasis, immune regulation, and tissue regeneration (Lin & Leonard, 2000; O'Shea et al., 2015). While its normal activity is critical for physiological homeostasis, its dysregulation is strongly implicated in tumor progression. These multifaceted functions have established STAT5 as a compelling candidate for therapeutic intervention (Hennighausen & Robinson, 2008; Huang et al., 2023). Despite the well-established roles of STAT5 in vertebrate models, its functions in invertebrates with high regenerative capacity remain largely unexplored.

In this study, we identified and characterized *Djstat5*, a STAT5-like gene in the planarian *Dugesia japonica*. Spatiotemporal expression profiling and RNA interference (RNAi)-mediated knockdown demonstrated that *Djstat5* is dynamically expressed during regeneration and plays a functional role in this process. Mechanistically, *Djstat5* appears to modulate both neoblast proliferation and apoptosis, potentially through regulation of *Djnlrc3*, a gene implicated in inhibiting the PI3K signaling pathway. These findings suggest that *Djstat5* contributes to stem cell-mediated regeneration in planarians and provide new insight into conserved STAT-regulated regenerative signaling pathways.

MATERIALS AND METHODS

Planarian husbandry

A clonal strain of *D. japonica*, originally collected from Qinling, China, was maintained as previously described (Zheng et al., 2021) and used in all experiments. Planarians measuring 5–8 mm in body length were starved for at least one week prior to experimentation. To examine regeneration dynamics, animals were transversely amputated into three fragments—anterior, trunk, and posterior—relative to the pharyngeal region, and allowed to regenerate under controlled conditions.

Bioinformatics analysis

The STAT5 protein sequences from multiple species were retrieved from the NCBI database (https://www.ncbi.nlm.nih.gov). A multiple sequence alignment was performed using the MEGA software (v.11.0.13). A phylogenetic tree was constructed via the neighbor-joining method, with branch support evaluated by 1 000 bootstrap replicates. The resulting phylogenetic tree was visualized using the ChiPlot interactive tool (https://www.chiplot.online/tvbot.html) (Xie et al., 2023).

RNA interference

RNAi was performed via oral delivery of bacterially expressed double-stranded RNA (dsRNA) according to established methodologies (Zeng et al., 2013). Gene-specific fragments of *Djstat5* and *Djnlrc3* were cloned into the L4440 vector (BioVector NTCC, China). The recombinant RNAi vector was transformed into HT115 competent cells (BioVector NTCC, China), and dsRNA expression was induced with 0.4 mmol/L Isopropyl β-D-thiogalactopyranoside (IPTG) (Amresco, United States). For RNAi treatment, bacterial pellets expressing the target dsRNA were mixed with liver homogenate and fed to planarians. Control animals received similarly prepared dsRNA targeting *EGFP*. RNAi efficiency was evaluated by quantitative real-time PCR (qRT-PCR) 72 h after the final feeding. For regeneration and homeostasis experiments, planarians were subjected to 5 and 15 rounds of RNAi feeding, respectively.

Treatment with chemical inhibitors

The STAT5-specific inhibitor STAT5-IN-1 (Selleck, United States) was dissolved in DMSO and used at a series of gradient concentrations. After amputation, planarians were allowed to regenerate in STAT5-IN-1 solution until the entire regeneration cycle was completed. To ensure sustained inhibitor activity, the drug solution was replaced every three days. For homeostasis studies, planarians were continuously exposed to STAT5-IN-1 for 20 days.

Reverse transcription and quantitative real-time PCR analysis

Total RNA was extracted from planarian samples using RNAiso Plus (Takara, Japan), and 1 μg of RNA was reverse transcribed using the Transcriptor First Strand cDNA Synthesis Kit (Roche, Germany). qRT-PCR was performed with SYBR Premix Ex Taq (Roche, Germany) on a QuantStudio 3 Real-Time PCR System (Applied Biosystems, United States). The cycling conditions were: 95°C for 10 s, followed by 40 cycles of 95°C for 10 s, 60°C for 10 s, and 72°C for 10 s. Primer sequences are listed in Supplementary Table S1.

Western blot analysis

For all experiments, total and nuclear protein samples were collected from regenerating tail fragments at 48 hpa. Total proteins were extracted from planarian samples using RIPA buffer (Proandy, China) supplemented with a protease inhibitor cocktail (Proandy, China) and phosphatase inhibitors (Proandy, China). Nuclear proteins were extracted using a commercial nuclear protein extraction kit (Beyotime, China) and quantified with a BCA Protein Assay Kit (Thermo, United States). Equal amounts of protein were separated by SDS-PAGE and transferred to PVDF membranes (Millipore, United States). Membranes were blocked with 10% skim milk for 1 h at room temperature, incubated with primary antibodies overnight at 4°C, and then with HRP-conjugated secondary antibodies. Signals were detected using BeyoECL Plus (Beyotime, China), and β-actin (1:10 000, Abmart, China) and Histone H3 (1:2 000, Cell Signaling Technology, United States) served as loading controls for total and nuclear proteins, respectively. Quantification of protein bands was performed using ImageJ software. Detailed information on all antibodies used in this study is provided in Supplementary Table S2.

In situ hybridization

Whole-mount *in situ* hybridization (WISH) and fluorescent *in situ* hybridization (FISH) were performed based on a slightly modified protocol previously described (Pearson et al., 2009). Digoxigenin-labeled antisense RNA probes were synthesized using an *in vitro* transcription kit (Roche, Germany).

Planarians were treated with 2% HCl for 5 min at room temperature to remove mucus, incubated in 5% N-acetylcysteine, and fixed in 4% paraformaldehyde. After bleaching and rehydration, specimens were digested with proteinase K (10 μg/mL, Merck, Germany) and re-fixed in 4% paraformaldehyde. Hybridization was performed at 56°C overnight with 1 ng/μL Digoxigenin-labeled probes after pre-hybridization, followed by washes in pre-warmed gradient SSC solution. For WISH, samples were blocked and incubated overnight at 4°C with anti-Digoxigenin-AP antibody (1:4 000, Roche, Germany) and developed using NBT/BCIP (Roche, Germany). For FISH or double FISH analyses, samples were incubated overnight in anti-Digoxigenin-POD (1:100, Roche, Germany) and anti-fluorescein-POD (1:100, Roche, Germany), developed using Cy3-tyramide (1:500, MedChemExpress, United States) and fluorescein-tyramide (1:500, MedChemExpress, United States) solution.

Whole-mount immunostaining

Planarians were pre-treated in ice-cold 2% HCl for 2–5 min and fixed in 4% paraformaldehyde. After rinsing in cold methanol for 1 h, samples were bleached overnight in methanol with 6% H_2O_2 at 4°C, rehydrated, and blocked for 1 h in 0.6% BSA and 0.45% fish gelatin in PBSTx. Primary antibodies used included anti-phospho-Histone H3 (1:200, Millipore, United States) and anti-SYNORF1 (1:25, DSHB, United States), followed by secondary antibodies goat anti-mouse IgG (1:200, Millipore, United States) and goat anti-rabbit IgG-Alexa Fluor 488 (1:200, Abcam, United Kingdom). Incubations were performed overnight at 4°C. Fluorescence signals were acquired using an FV3000 confocal microscope (Olympus, Japan) and analyzed with ImageJ. Antibody details are listed in Supplementary Table S2.

Whole-mount TUNEL

A whole-mount TUNEL assay was performed as described (Pellettieri et al., 2010). After fixation, the planarians were treated with 1% SDS for 20 min for permeabilization, followed by overnight bleaching in methanol containing 6% H_2O_2. The TUNEL assay was then conducted utilizing the One Step TUNEL Apoptosis Assay Kit (Beyotime, China). TUNEL signals were imaged using an FV3000 confocal microscope (Olympus, Japan) and ImageJ software (v.1.54p).

Measurements of planaria and image processing

Live and WISH images were acquired using an EOS 600D camera (Canon, Japan) mounted on an SZX10 stereomicroscope (Olympus, Japan). Fluorescent Z-stack images were obtained with an FV3000 confocal microscope (Olympus, Japan) and processed using Fiji (ImageJ). H3P-positive cells were counted from Z-stacks with a consistent number of optical sections within defined regions. Blastema size was quantified by measuring regenerated blastema length and normalizing it to trunk length using Fiji. At each time point, the blastema-to-body length ratio in RNAi-treated animals was compared to that of controls.

RNA-seq and data analysis

Total RNA was extracted using TRIzol reagent (Invitrogen, United States), and RNA integrity was assessed with a Bioanalyzer 2100 (Agilent, United States). High-quality RNA samples (RIN>7.0) were used for RNA sequencing (RNA-seq) library preparation. Poly(A) RNA was purified using oligo (dT) magnetic beads, fragmented, and reverse-transcribed into cDNA. After second-strand synthesis, end repair, A-tailing, and adapter ligation, libraries with an average insert size of approximately 300 bp were PCR-amplified and purified. Paired-end sequencing (2×150 bp) was performed on an Illumina NovaSeq™ 6000 platform (LC Bio Technology Co., Ltd., Hangzhou, China). Clean reads were obtained using fastp v.0.23.1 (Chen et al., 2018) to remove adapters and low-quality sequences. *De novo* transcriptome assembly was conducted using Trinity v.2.4.0 (Grabherr et al., 2011), generating a set of unigene sequences. For annotation, all unigenes were compared against public databases including Gene Ontology (GO), Kyoto Encyclopedia of Genes and Genomes (KEGG), and SwissProt, and the best-matching gene information was assigned as the annotation for each unigene. Transcript abundance was estimated as TPM using Salmon, and differentially expressed genes (DEGs) were identified with edgeR using the criteria $|\log_2\text{fold change}|\geq 1$, $FDR<0.05$. After obtaining annotation information, GO and KEGG enrichment analyses of the DEGs were performed using a hypergeometric test, with all annotated unigenes used as the background gene set. The enrichment *P*-value was calculated as:

$$P = 1 - \sum_{i=0}^{m-1} \frac{\binom{M}{i}\binom{N-M}{n-i}}{\binom{N}{n}} \quad (1)$$

where N is the number of annotated genes, n is the number of DEGs within N, M is the number of genes associated with a specific GO term or KEGG pathway, and m is the number of DEGs within M. The adjusted *P*-values were calculated using the Benjamini-Hochberg method. Visualization of volcano plots and GO/KEGG enrichment results was performed using the ChiPlot web tool (https://www.chiplot.online/tvbot.html).

Statistical analysis

Data are presented as mean±SEM. Statistical comparisons were performed using Student's *t*-test in SPSS 21.0. In the figures, ns: Not significant; *: $P<0.05$; **: $P<0.01$; ***: $P<0.001$.

RESULTS

Identification and expression analysis of *Djstat5* during planarian regeneration

A STAT-like gene was cloned from *D. japonica*, and the predicted protein contains a conserved DNA-binding domain (DBD) and a Src homology 2 (SH2) domain (Figure 1A). Phylogenetic analysis further showed that this protein clusters with other STAT5 homologs among STAT family members (Figure 1B). Based on these features, the gene was designated *Djstat5*. The expression pattern of *Djstat5* in both intact and regenerating planarians was examined using WISH. In uninjured animals, *Djstat5* was broadly expressed, with notable enrichment in the parenchyma and cerebral nervous system (Figure 1C). Additionally, analysis of single-cell transcriptomic data from a previously established database by Zeng et al. (2018) showed that *Smed-stat5* (Smed ID: SMED30003001), the homolog of *Djstat5* in *Schmidtea mediterranea*, is highly expressed in neoblast clusters and their progeny (Figure 1D). To validate *Djstat5* expression in neoblasts, double FISH was performed for *Djstat5* and *DjpiwiA*, a well-established neoblast marker (Zhen et al., 2023). This analysis revealed partial colocalization of *Djstat5* transcripts with *DjpiwiA* in the prepharyngeal region (Figure 1E), indicating that *Djstat5* is expressed in mitotically active stem cells. To further confirm this, we used the histone H2B (*Djh2b*) RNAi model to deplete neoblasts in planarians. Five days after the final feeding, *Djh2b* RNAi animals showed

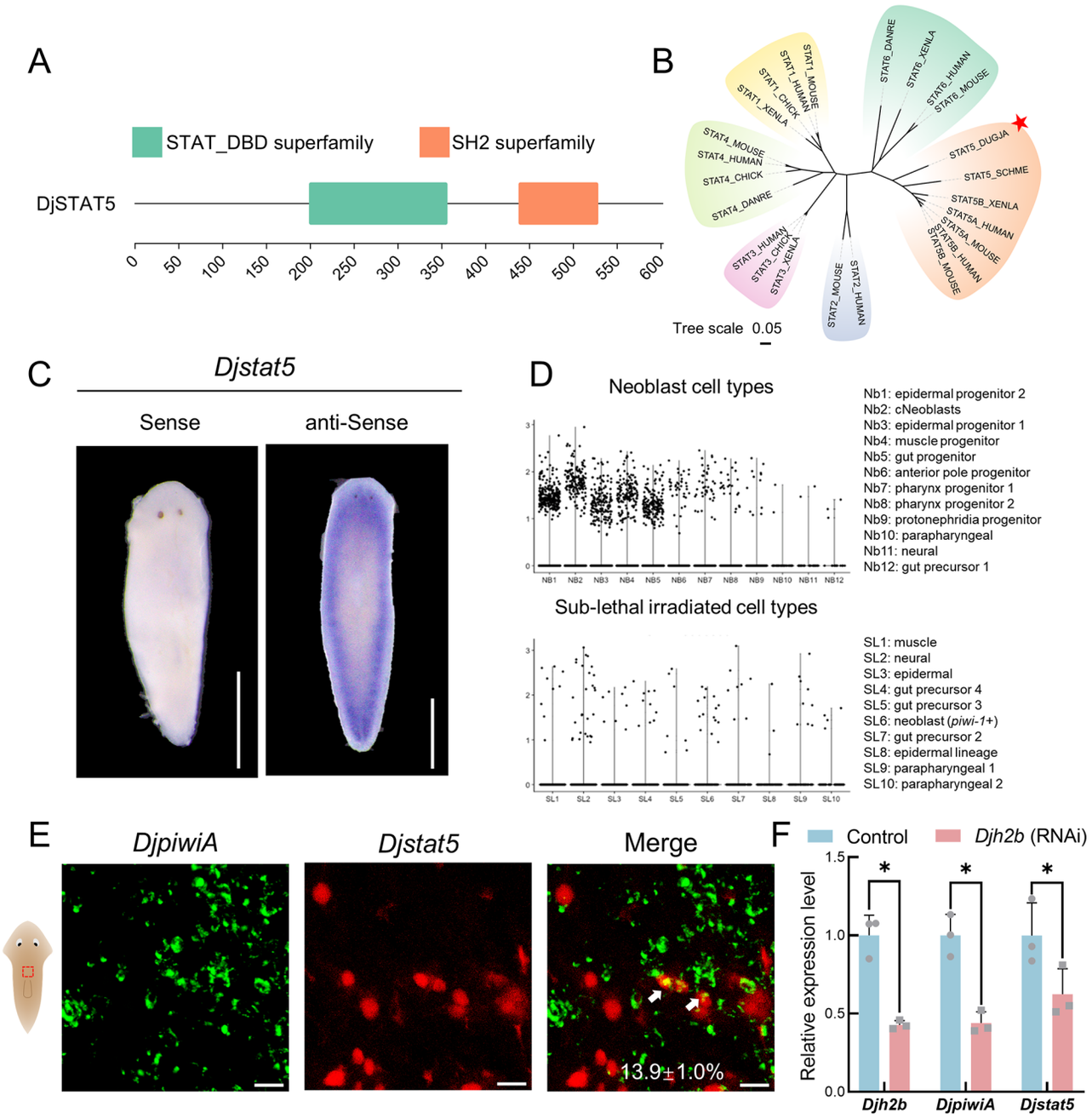

Figure 1 Evolutionary and structural characterization of *Djstat5* and its spatiotemporal expression pattern in intact planarians

A: Conserved domain architecture of the DjSTAT5 protein predicted using the NCBI Conserved Domain Database. The DBD and SH2 domains are indicated in green and orange, respectively. B: Phylogenetic tree constructed from representative STAT protein sequences, grouped into six clades corresponding to STAT1 (yellow), STAT2 (blue), STAT3 (purple), STAT4 (light green), STAT5 (orange), and STAT6 (green). C: WISH analysis of *Djstat5* expression in intact planarians. Scale bar=1 mm. D: Violin plots of *Smed-stat5* expression across neoblast and sublethally irradiated cell clusters from published single-cell transcriptomic data. E: Double FISH for *Djstat5* (red) and *DjpiwiA* (green). The ratios indicate the percentage of *Djstat5*$^+$ *DjpiwiA*$^+$ cells in *Djstat5*$^+$ cells. *n*=3. White arrows indicate double-positive cells. Scale bar=20 μm. F: qRT-PCR analysis of *Djh2b*, *DjpiwiA*, and *Djstat5* expression following *Djh2b* RNAi. Expression levels were normalized to the reference gene *Djβ-actin*. *: $P<0.05$.

a marked reduction in *DjpiwiA* expression and a concomitant decrease in *Djstat5* levels (Figure 1F), suggesting that *Djstat5* expression depends on the presence of neoblasts.

During regeneration, *Djstat5* expression gradually increased and became strongly enriched in the blastema at 2 and 3 days post-amputation (dpa) (Figure 2A). To corroborate these findings, we isolated blastema samples for qRT-PCR analysis. The results aligned with the WISH data, showing increased expression during early regeneration (Figure 2B, C). These spatiotemporal expression patterns indicate that *Djstat5* may play a potential role in blastema formation during regeneration.

Djstat5 is required for missing-tissue regeneration

To determine the functional role of *Djstat5* in planarian regeneration, RNAi knockdown was performed as illustrated in Figure 3A. Efficient depletion of *Djstat5* was confirmed by qRT-PCR (Figure 3B), and levels of nuclear phosphorylated Stat5 (p-Stat5) were markedly reduced (Figure 3C, D). Compared with control animals, *Djstat5* RNAi planarians

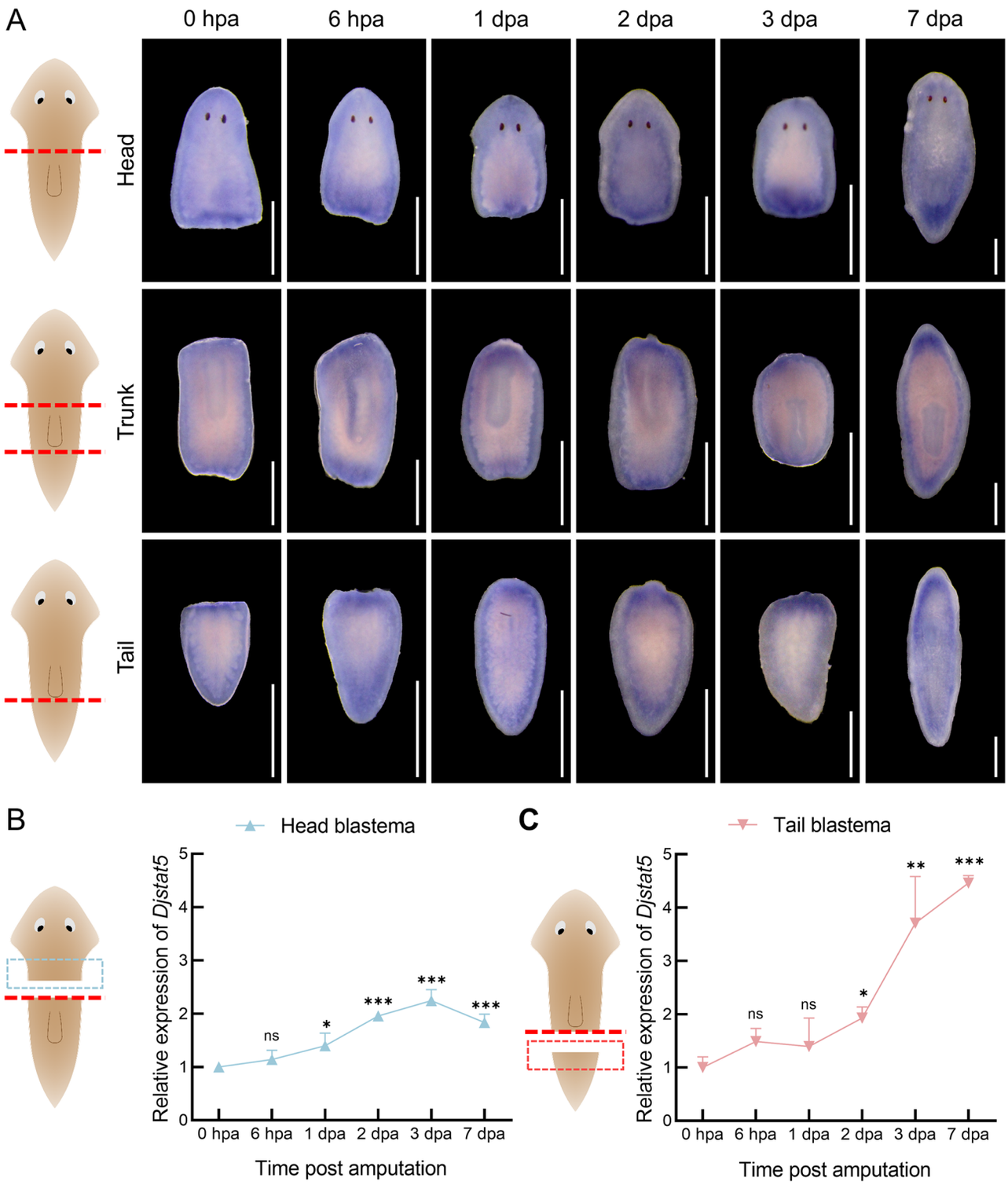

Figure 2 Spatiotemporal expression pattern of *Djstat5* during planarian regeneration

A: WISH analysis of *Djstat5* expression at various time points during regeneration. Scale bar=1 mm. B, C: qRT-PCR analysis of *Djstat5* expression in isolated blastemas from head (B) and tail (C) fragments during regeneration, with the respective blastema regions outlined in blue and red boxes. Expression levels were normalized to the reference gene *Djβ-actin*. ns: Not significant; *: $P<0.05$; **: $P<0.01$; ***: $P<0.001$.

exhibited significantly smaller blastemas by 3 dpa and failed to regenerate eyespots by 7 dpa (Figure 3E, F). Immunostaining using the anti-SYNORF1 antibody (a neuronal marker) further revealed impaired brain regeneration in *Djstat5* RNAi animals (Figure 4A). WISH analysis showed incomplete regeneration of both the anterior intestinal branches and the pharynx in *Djstat5* RNAi animals (Figure 4B). These results indicate that *Djstat5* is essential for the regeneration of multiple internal tissues in planarians.

To elucidate the mechanisms underlying these regeneration defects, we examined cell proliferation and apoptosis following amputation. In planarians, neoblasts are the only proliferative cells, showing a systemic mitotic peak at 6 hpa and a localized peak at 48 hpa (Wenemoser & Reddien, 2010). Using anti-

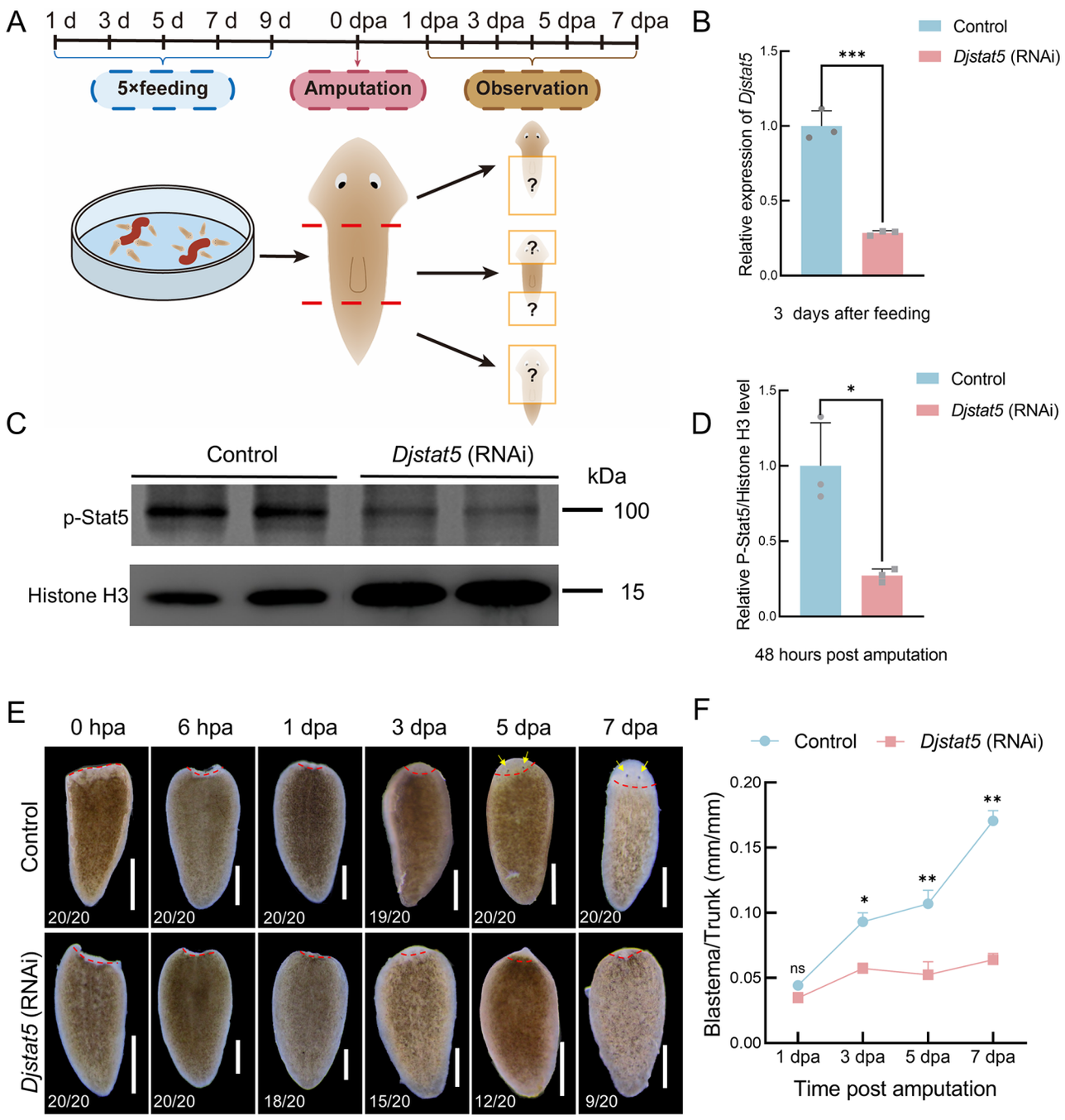

Figure 3 Effects of *Djstat5* knockdown on planarian regeneration

A: Schematic of the RNAi feeding schedule and regeneration assay. Animals were subjected to five rounds of feeding with *Djstat5* dsRNA-containing liver paste every other day, followed by amputation three days after the final feeding to examine regenerative phenotypes. B: qRT-PCR validation of *Djstat5* knockdown efficiency following RNAi treatment. Expression levels were normalized to *Djβ-actin*. C: Western blot analysis of phosphorylated STAT5 (p-Stat5) in nuclear extracts from tail fragments at 48 hpa. Histone H3 was used as a nuclear loading control. D: Quantification of p-Stat5 protein levels from panel (C), measured by grayscale band intensity and normalized to Histone H3. E: Representative dorsal views of regenerating tail fragments from control and *Djstat5* RNAi animals at indicated time points post-amputation. Newly regenerated photoreceptors are indicated by yellow arrows. Scale bar=1 mm. F: Quantification of blastema length from panel (E), normalized to trunk length. ns: Not significant; *: P<0.05; **: P<0.01; ***: P<0.001.

H3P immunostaining to label mitotic cells, we found that *Djstat5* RNAi significantly reduced H3P-positive cells, indicating an impairment in proliferation (Figure 4C, D). Apoptosis, essential for tissue remodeling, occurs in two waves: early (6 hpa) near the wound and late (48 hpa) body-wide (Pellettieri et al., 2010). TUNEL assays revealed fewer apoptotic cells in *Djstat5* RNAi animals at both time points compared to controls (Figure 4E, F). Taken together, these findings demonstrate that *Djstat5* plays a critical role in regulating both neoblast proliferation and apoptosis, and is essential for proper tissue regeneration in planarians.

Validation of *Djstat5* function via STAT5-IN-1 inhibitor treatment

Given the phenotypic and cellular defects observed following *Djstat5* knockdown, we next asked whether these effects were

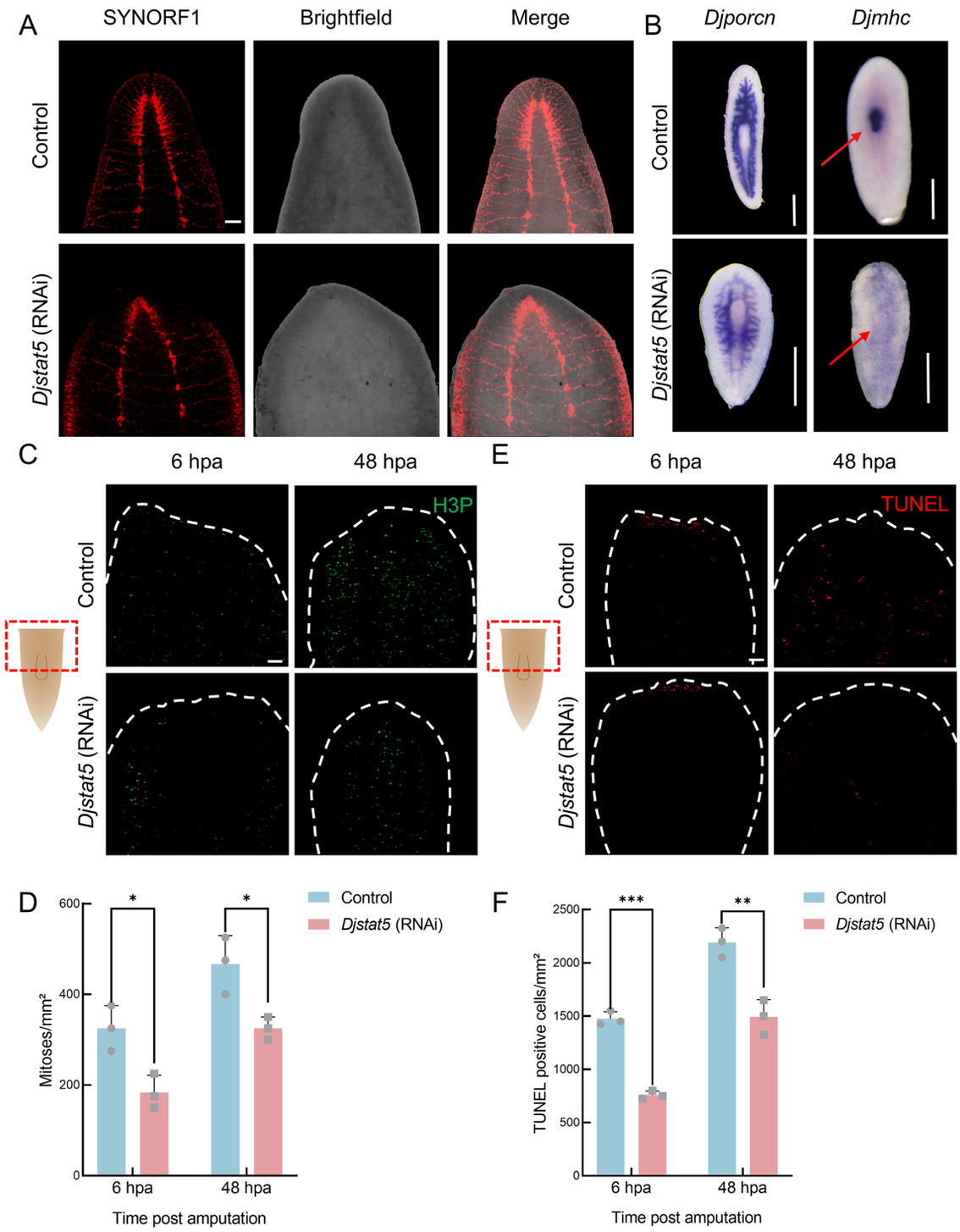

Figure 4 *Djstat5* knockdown impairs tissue regeneration and disrupts cell proliferation and apoptosis in planarians

A: Immunostaining of the regenerated central nervous system at 7 dpa using an anti-SYNORF1 antibody. Scale bar=100 μm. B: WISH analysis of regenerated tissues in control and *Djstat5* RNAi animals at 7 dpa, using the intestinal marker *Djporcn* and the pharyngeal marker *Djmhc*. Scale bar=1 mm. C, D: Representative H3P staining images (C) and quantification (D) of mitotic cells (green) in regenerating tail fragments at 6 and 48 hpa. Scale bar=100 μm. E, F: Representative TUNEL staining images (E) and quantification (F) of apoptotic nuclei (red) in tail fragments at 6 and 48 hpa. Scale bar=100 μm. *: P<0.05; **: P<0.01; ***: P<0.001.

directly attributable to STAT5 activity. To address this, we treated planarians with STAT5-IN-1, a small-molecule inhibitor that targets the SH2 domain of STAT5 (Li et al., 2021; Müller et al., 2008). The treatment scheme is outlined in Supplementary Figure S1A. Briefly, planarians were amputated and allowed to regenerate in a gradient concentration of STAT5-IN-1. The results showed that concentrations ranging from 20 to 60 μmol/L caused regeneration defects, and 60 μmol/L produced the most severe and consistent regeneration failure (Supplementary Figure S1B). Statistical results showed that 60 μmol/L produced the most severe and consistent regeneration failure (Supplementary Figure S1C), and this concentration was therefore selected for all subsequent experiments. Western

blot analysis confirmed that STAT5-IN-1 treatment markedly reduced the levels of p-Stat5 in planarians (Supplementary Figure S1D, E).

Regeneration of tail fragments in 60 μmol/L STAT5-IN-1 closely resembled the phenotype of *Djstat5* RNAi animals, with markedly reduced blastema formation and failure to regenerate eyespots (Supplementary Figure S2A, B). Immunostaining and WISH results further revealed incomplete regeneration of the brain, intestine, and pharynx in inhibitor-treated planarians (Supplementary Figure S2C, D). At the cellular level, STAT5-IN-1 treatment significantly reduced both cell proliferation and apoptosis (Supplementary Figure S2E–H), mirroring the effects observed in *Djstat5* RNAi planarians.

We also examined whether prolonged loss of STAT5 function affected planarian homeostasis. Neither long-term RNAi (15 rounds of RNAi) nor continuous inhibitor immersion (20 days) induced obvious homeostatic defects (Supplementary Figure S3A–C). WISH results confirmed that the intestine, brain, pharynx and epidermis of planarians remained normal under these conditions (Supplementary Figure S3D–O). In summary, pharmacological inhibition of STAT5 recapitulates the regeneration-specific defects observed in *Djstat5* RNAi animals, further supporting the essential role of *Djstat5* in planarian regeneration.

Transcriptomic identification of *Djstat5* downstream targets

To examine the transcriptomic changes caused by *Djstat5* knockdown, RNA sequencing (RNA-seq) was performed on head-regenerating blastema tissues from control and *Djstat5* RNAi animals to identify genes potentially regulated, directly or indirectly, by *Djstat5* (Figure 5A). A total of 350 differentially expressed genes (DEGs) were identified, including 246 significantly upregulated and 104 downregulated genes (Figure 5B). To gain insight into the molecular pathways downstream of *Djstat5*, we performed KEGG and GO enrichment analyses. KEGG analysis revealed significant enrichment in several core metabolic pathways, including oxidative phosphorylation, glycolysis/gluconeogenesis, galactose metabolism, and purine metabolism (Figure 5C), implying a potential role for *Djstat5* in modulating energy production and metabolic reprogramming during regeneration.

GO enrichment analysis further highlighted biological processes related to stem cell regulation and tissue development, with enriched terms such as “negative regulation of fibroblast proliferation”, “negative regulation of PI3K signaling”, “cell fate determination”, and “Wnt signaling pathway” (Figure 5D). Among these, the PI3K pathway is of particular interest, as it has been previously shown to be critical for neoblast proliferation and regeneration in planarians (Peiris et al., 2012, 2016; Zheng et al., 2021). Western blot analysis further confirmed that the activity of PI3K signaling is significantly repressed after *Djstat5* knockdown (Figure 5E, F). This prompted our investigation into *Djnlrc3*, a gene that exhibits significant upregulation in *Djstat5* RNAi animals and is predicted to function as a negative regulator of PI3K signaling.

To validate the RNA-seq results, qRT-PCR analysis was conducted on a subset of DEGs, which confirmed the expression changes observed in the transcriptomic data (Figure 5G). Collectively, these results position *Djnlrc3* as a potential downstream target of *Djstat5* and suggest its involvement in the regulatory network controlling planarian regeneration.

Djstat5* promotes regeneration by repressing *Djnlrc3

Double FISH analysis indicated partial colocalization of *Djnlrc3* transcripts with *Djstat5* (Figure 6A). To further characterize their spatial co-expression patterns across different anatomical regions, additional representative dFISH images are presented in Supplementary Figure S4. To determine whether the regeneration defects observed in *Djstat5* RNAi animals are mediated through *Djnlrc3*, double RNAi experiments were performed. After five rounds of RNAi, the expression levels of both genes were significantly reduced, as confirmed by qRT-PCR (Figure 6B). Notably, simultaneous knockdown of *Djstat5* and *Djnlrc3* effectively rescued the regeneration defects, resulting in restored blastema formation and overall morphological recovery (Figure 6C, D). Immunostaining and WISH results further revealed that the rescue occurred across multiple tissues, including the nervous system, intestine, and pharynx (Figure 6E, F).

We next assessed whether this phenotypic rescue was accompanied by recovery at the cellular level. Dual knockdown of *Djstat5* and *Djnlrc3* partially restored mitotic activity in *Djstat5* RNAi animals, as evidenced by an increase in H3P-positive cells (Figure 7A, B). Similarly, TUNEL assays indicated that apoptosis levels were also partially recovered following the double knockdown (Figure 7C, D). However, single *Djnlrc3* RNAi alone did not induce significant regeneration defects (Figure 6, 7), suggesting that its function becomes critical primarily in the context of *Djstat5* deficiency.

Taken together, these results indicate that *Djstat5* promotes planarian regeneration by repressing *Djnlrc3*, a putative negative regulator of PI3K signaling, and that the *Djstat5*–*Djnlrc3* regulatory axis modulates both neoblast proliferation and apoptosis, thereby supporting effective tissue regeneration (Figure 7E).

DISCUSSION

STAT5 is a pivotal intracellular signaling mediator involved in immune regulation, tissue morphogenesis, and injury-induced regeneration. In line with its conserved functions, we identified the STAT5 homolog *Djstat5* in *D. japonica* and examined its role in planarian regeneration. Combining single-cell transcriptomic analysis with double FISH, we observed that *Djstat5* was partially co-expressed with the neoblast marker *DjpiwiA*, indicating its expression in a subpopulation of neoblasts. Functional studies using RNAi demonstrated that *Djstat5* is required for maintaining neoblast mitotic activity during blastema formation, underscoring its essential role in regenerative progression.

Structurally, STAT5 proteins are characterized by several conserved domains, including an N-terminal domain, a DBD, a SH2 domain, and a C-terminal transcriptional activation domain (Xin et al., 2020). Sequence alignment of *Djstat5* revealed high amino acid conservation within the DBD and SH2 domains, consistent with STAT5 homologs in other metazoans (Figure 1B). In canonical JAK/STAT signaling, the SH2 domain recognizes phosphotyrosine residues on activated cytokine receptors such as EGFR (Philips et al., 2022). Following activation, STAT5 dimerizes through SH2-phosphotyrosine interactions, translocates to the nucleus, and binds DNA to regulate transcription.

Spatiotemporal profiling revealed strong enrichment of *Djstat5* expression in the blastema as early as 2 dpa (Figure 2A–C), indicating its involvement in early regenerative signaling (Wang et al., 2022). This response is consistent with the view that injury activates broad signaling cascades that

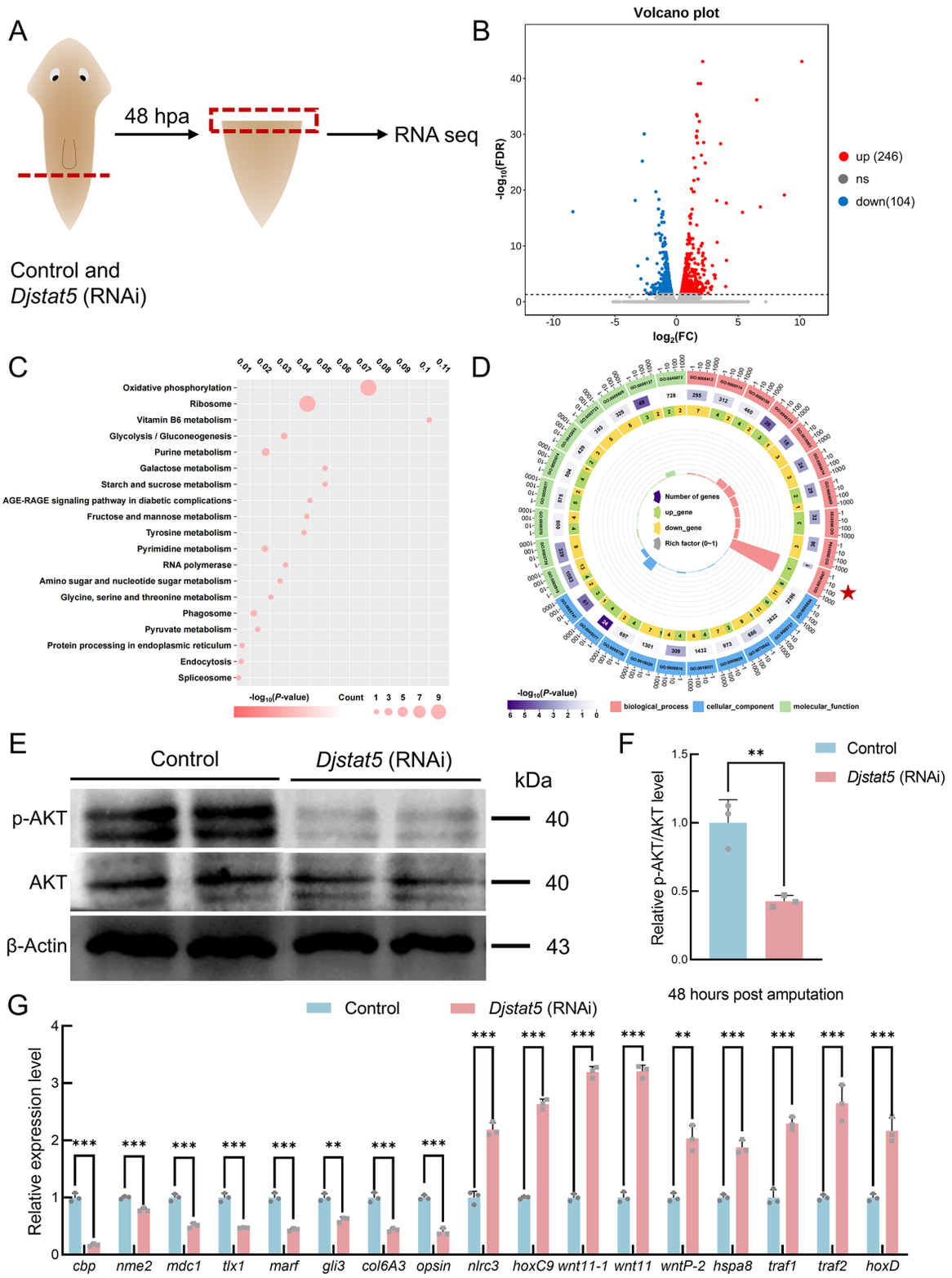

Figure 5 Transcriptomic analysis of *Djstat5*-regulated genes

A: Experimental workflow for RNA-seq sample collection from regenerating head blastemas (red box). B: Volcano plot showing differentially expressed genes (DEGs) between control and *Djstat5* RNAi samples. C: Enrichment analysis of DEGs in selected KEGG pathways. Bubble color reflects the $-\log_{10}$(*P*-value), with darker shades indicating greater significance; bubble size corresponds to the number of DEGs in each pathway. D: GO enrichment analysis of DEGs presented in a circular layout. Rings from outer to inner indicate: GO category, total gene count ($-\log_{10}$(*P*-value) by color intensity), counts of up-regulated (green) and down-regulated (yellow) DEGs, and Rich Factor. The term "negative regulation of PI3K signaling" is marked by a red star. E: Western blot analysis of phosphorylated AKT (p-AKT) in total protein extracts from tail fragments at 48 hpa. AKT was used as a loading control. F: Quantification of p-AKT protein levels from panel (E), measured by grayscale band intensity and normalized to AKT. G: qRT-PCR validation of selected DEGs identified in the RNA-seq analysis. Expression levels were normalized to *Djβ-actin*. **: $P<0.01$; ***: $P<0.001$.

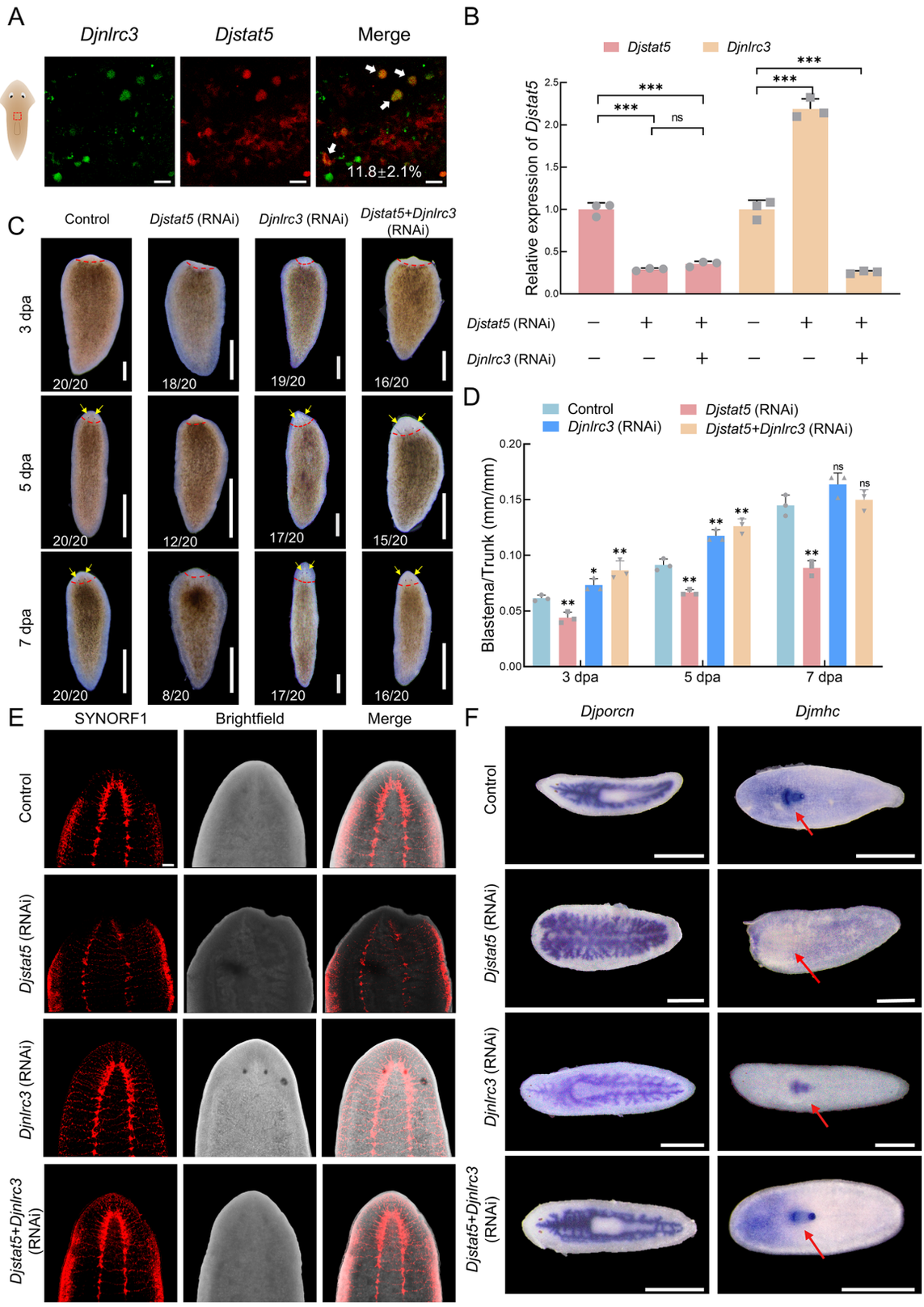

Figure 6 *Djstat5* regulates regeneration through *Djnlrc3*

A: Double FISH for *Djstat5* (red) and *Djnlrc3* (green). The ratios indicate the percentage of *Djstat5*$^{+}$ *Djnlrc3*$^{+}$ cells in *Djstat5*$^{+}$ cells. *n*=3. White arrows indicate double-positive cells. Scale bar=20 μm. B: qRT-PCR analysis of *Djstat5* and *Djnlrc3* transcript levels following RNAi. Expression levels were normalized to *Djβ-actin*. C: Dorsal views of regenerating tail fragments from control, *Djstat5* RNAi, *Djnlrc3* RNAi, and *Djstat5*+*Djnlrc3* RNAi animals at 3 dpa, 5 dpa, and 7 dpa. Yellow arrows indicate newly regenerated photoreceptors. Scale bar=1 mm. D: Quantitative analysis of blastema length normalized to trunk length (measured from samples in panel C) at the indicated time points, compared to controls. E: Immunostaining of the regenerated central nervous system at 7 dpa using an anti-SYNORF1 antibody. Scale bar=100 μm. F: WISH analysis of regenerated intestinal (*Djporcn*) and pharyngeal (*Djmhc*) tissues at 7 dpa. Scale bar=1 mm. ns: Not significant; *: P<0.05; **: P<0.01; ***: P<0.001.

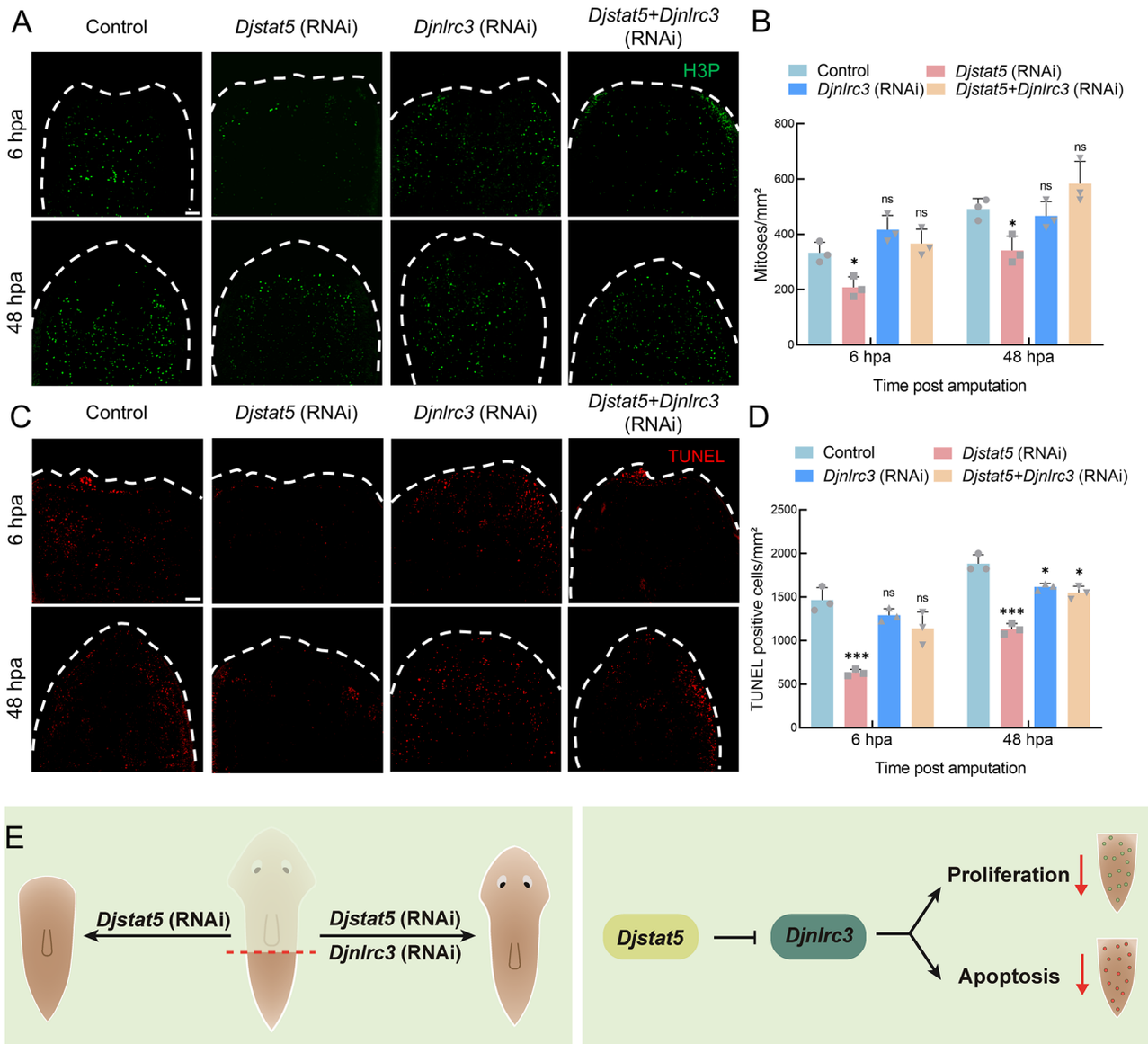

Figure 7 *Djnlrc3* knockdown alleviates proliferation and apoptosis defects caused by *Djstat5* loss

A, B: Representative images (A) and quantification (B) of H3P-stained mitotic cells (green) in regenerating tail fragments from *Djstat5* RNAi, *Djnlrc3* RNAi, and dual RNAi animals, compared to controls at 6 and 48 hpa. Scale bar=100 μm. C, D: Representative TUNEL staining (C) and quantification (D) of apoptotic nuclei (red) under identical comparisons. Scale bar=100 μm. E: Proposed model: *Djstat5* promotes planarian regeneration by repressing *Djnlrc3*, thereby coordinating neoblast proliferation and apoptosis. ns: Not significant; *: $P<0.05$; ***: $P<0.001$.

diverge into regeneration programs, depending on the extent of tissue loss (Wurtzel et al., 2015). Notably, the cellular hallmark of regeneration initiation—the secondary mitotic wave of neoblasts observed at 2–3 dpa (Wenemoser & Reddien, 2010)—coincides with a marked spatial shift of *Djstat5* expression from the wound edge to the forming blastema. Given its expression in neoblasts and dynamic regulation, *Djstat5* may function as a context-specific mediator that participates in orchestrating stem cell responses during blastema formation.

Our functional analysis supports a conserved role for STAT signaling in regulating regeneration across metazoans. In *Drosophila*, STAT92E is essential for intestinal stem cell proliferation and epithelial repair following damage (Jiang et al., 2009; Verghese & Su, 2016). In mammals, STAT5 plays prominent roles in promoting mucosal healing (Gilbert et al., 2012), enhancing intestinal stem cell activity under inflammatory stress (Surbek et al., 2021), and maintaining stem cell homeostasis in both hematopoietic (Williams et al., 2025) and hepatic systems (Fu et al., 2016). Interestingly, in skeletal tissues, STAT5 exhibits dual roles, either promoting osteoblast differentiation (Dieudonne et al., 2013; Kamalakar et al., 2024) or inhibiting bone healing under fracture conditions (Lee et al., 2018), illustrating the context-dependent nature of STAT5 signaling across tissue types. These findings converge on a shared function of STAT5 in stem cell activation and tissue restoration.

Because RNA-seq captures both the direct and indirect consequences of *Djstat5* depletion, the identified DEGs likely represent a mixture of primary and secondary regulatory changes rather than direct transcriptional targets. Transcriptomic profiling of *Djstat5* RNAi animals identified *Djnlrc3* as a putative downstream effector. *Djnlrc3*, a member of the NOD-like receptor family, has been reported in mammalian systems to negatively regulate the PI3K-AKT-mTOR pathway by interfering with PI3K subunit interactions

and attenuating proliferative signaling (Karki et al., 2016, 2017; Zheng et al., 2021). These pathways are crucial for planarian regeneration, particularly in maintaining neoblast proliferation and blastema growth (Iglesias et al., 2019; Kang et al., 2021; Peiris et al., 2016). In our study, double RNAi experiments showed that co-knockdown of *Djstat5* and *Djnlrc3* significantly rescued the mitotic and morphological defects caused by *Djstat5* loss, suggesting that *Djstat5* promotes regeneration, at least in part, by suppressing *Djnlrc3*-mediated inhibitory signaling. This is consistent with findings in vertebrates where NLRC3 acts as a brake on epithelial proliferation and its deletion enhances wound healing or tumorigenesis through hyperactivation of PI3K-mTOR and suppression of p53 signaling (Karki et al., 2016; Qin et al., 2022). Notably, single *Djnlrc3* RNAi alone did not induce significant regeneration defects, indicating that its function becomes critical primarily in the context of *Djstat5* deficiency.

Mechanistically, STAT5 proteins are well-characterized transcriptional regulators that bind to promoter regions and modulate gene expression through recruitment of co-activators or co-repressors. The co-localization of *Djstat5* with *Djnlrc3* raises the possibility that *Djstat5* transcriptionally represses *Djnlrc3*, although whether this regulation is direct or indirect remains to be determined. Consistent with this notion, our Western blot analyses showed that p-AKT levels were significantly reduced in *Djstat5* RNAi animals (Figure 5E, F), suggesting a potential link between STAT5 activity and the PI3K/AKT signaling pathway. In mammals, NLRC3 inhibits phosphorylation of AKT and downstream effectors such as FoxO1 and FoxO3a, which are central to the control of cell proliferation and survival (Karki et al., 2017). NLRC3 also suppresses oncogenic drivers such as c-Myc and cyclin D1 via mTOR inhibition and promotes p53 stabilization by interacting with Hsp90-MDM2 complexes (Qin et al., 2022). These observations suggest that *Djstat5* may counteract *Djnlrc3* not only by modulating its transcription but also by coordinating broader regulatory modules that interface with the PI3K-AKT and p53 pathways. This interplay may constitute a conserved mechanism by which STAT5 facilitates stem cell activation and regenerative outgrowth following injury. However, further studies are needed to determine whether *Djstat5* directly represses the *Djnlrc3* promoter or acts through intermediate factors, and to explore its crosstalk with other injury-responsive pathways such as ERK, calcium signaling, and metabolic reprogramming.

In summary, our study establishes *Djstat5* as a key regulator of neoblast proliferation during planarian regeneration. By repressing *Djnlrc3*, a putative negative regulator of PI3K signaling, *Djstat5* promotes stem cell expansion and supports blastema formation. These findings highlight a conserved regulatory mechanism involving STAT signaling in invertebrate regeneration and suggest potential parallels with vertebrate systems.

DATA AVAILABILITY

All datasets were deposited in the Science Data Bank (DOI: 10.57760/sciencedb.j00139.00316), Genome Sequence Archive (GSA, accession No. CRA035155), and National Center for Biotechnology Information (NCBI BioProject ID PRJNA1194312) databases.

SUPPLEMENTARY DATA

Supplementary data to this article can be found online.

COMPETING INTERESTS

The authors declare that they have no competing interests.

AUTHORS' CONTRIBUTIONS

D.W., F.L.C., and Y.Y. conceived and designed the study. D.W., H.X.Z., J.Y.C., M.D.C., L.F.L., Y.J.N., Y.M.Q., W.J.X., and R.H.L. performed data analysis and interpreted the results. D.W., F.L.C., and Y.Y. wrote the manuscript. F.L.C., X.L., and Y.Y. supervised the study. H.X.Z., X.L., and Y.Y. acquired the funding. All authors read and approved the final version of the manuscript.

ACKNOWLEDGMENTS

The RNA libraries were sequenced on the Illumina NovaSeq™ 6000 platform by LC Bio Technology CO., Ltd (Hangzhou, China).

REFERENCES

Adell T, Cebrià F, Abril JF, et al. 2025. Cell death in regeneration and cell turnover: lessons from planarians and *Drosophila*. *Seminars in Cell & Developmental Biology*, **169**: 103605.

Awasthi N, Liongue C, Ward AC. 2021. STAT proteins: a kaleidoscope of canonical and non-canonical functions in immunity and cancer. *Journal of Hematology & Oncology*, **14**(1): 198.

Bassat E, Tanaka EM. 2021. The cellular and signaling dynamics of salamander limb regeneration. *Current Opinion in Cell Biology*, **73**: 117–123.

Chen JJ, Lei K. 2023. The known, unknown, and unknown unknowns of cell-cell communication in planarian regeneration. *Zoological Research*, **44**(5): 981–992.

Chen SF, Zhou YQ, Chen YR, et al. 2018. fastp: an ultra-fast all-in-one FASTQ preprocessor. *Bioinformatics*, **34**(17): i884–i890.

Chera S, Ghila L, Dobretz K, et al. 2009. Apoptotic cells provide an unexpected source of Wnt3 signaling to drive *Hydra* head regeneration. *Developmental Cell*, **17**(2): 279–289.

Dai YM, Cui CG, Jiao D, et al. 2025. JAK/STAT signaling as a key regulator of ferroptosis: mechanisms and therapeutic potentials in cancer and diseases. *Cancer Cell International*, **25**(1): 83.

Dieudonne FX, Sévère N, Biosse-Duplan M, et al. 2013. Promotion of osteoblast differentiation in mesenchymal cells through Cbl-mediated control of STAT5 activity. *Stem Cells*, **31**(7): 1340–1349.

Doddihal V, Mann FG Jr, Ross EJ, et al. 2024. A PAK family kinase and the Hippo/Yorkie pathway modulate WNT signaling to functionally integrate body axes during regeneration. *Proceedings of the National Academy of Sciences of the United States of America*, **121**(20): e2321919121.

Fu BS, Meng W, Zhao H, et al. 2016. GRAM domain-containing protein 1A (GRAMD1A) promotes the expansion of hepatocellular carcinoma stem cell and hepatocellular carcinoma growth through STAT5. *Scientific Reports*, **6**: 31963.

Ge XY, Han X, Zhao YL, et al. 2022. An insight into planarian regeneration. *Cell Proliferation*, **55**(9): e13276.

Gilbert S, Zhang RL, Denson L, et al. 2012. Enterocyte STAT5 promotes mucosal wound healing via suppression of myosin light chain kinase-mediated loss of barrier function and inflammation. *EMBO Molecular Medicine*, **4**(2): 109–124.

Grabherr MG, Haas BJ, Yassour M, et al. 2011. Full-length transcriptome assembly from RNA-Seq data without a reference genome. *Nature Biotechnology*, **29**(7): 644–652.

Han XS, Wang C, Guo FH, et al. 2019a. Neoblast-enriched zinc finger protein FIR1 triggers local proliferation during planarian regeneration. *Protein & Cell*, **10**(1): 43–59.

Han YC, Chen AZ, Umansky KB, et al. 2019b. Vitamin D stimulates cardiomyocyte proliferation and controls organ size and regeneration in Zebrafish. *Developmental Cell*, **48**(6): 853–863. e5.

Hennighausen L, Robinson GW. 2008. Interpretation of cytokine signaling through the transcription factors STAT5A and STAT5B. *Genes & Development*, **22**(6): 711–721.

Hu XY, Li J, Fu MR, et al. 2021. The JAK/STAT signaling pathway: from bench to clinic. *Signal Transduction and Targeted Therapy*, **6**(1): 402.

Huang ZW, Zhang XN, Zhang L, et al. 2023. STAT5 promotes PD-L1 expression by facilitating histone lactylation to drive immunosuppression in acute myeloid leukemia. *Signal Transduction and Targeted Therapy*, **8**(1): 391.

Iglesias M, Felix DA, Gutiérrez-Gutiérrez Ó, et al. 2019. Downregulation of mTOR signaling increases stem cell population telomere length during starvation of immortal planarians. *Stem Cell Reports*, **13**(2): 405–418.

Jia LY, Zheng HX, Feng JT, et al. 2025. Upregulation of protein O-GlcNAcylation levels promotes Zebrafish fin regeneration. *Molecular & Cellular Proteomics*, **24**(4): 100936.

Jiang HQ, Patel PH, Kohlmaier A, et al. 2009. Cytokine/Jak/Stat signaling mediates regeneration and homeostasis in the *Drosophila* midgut. *Cell*, **137**(7): 1343–1355.

Kamalakar A, Tobin B, Kaimari S, et al. 2024. Delivery of a Jagged1-PEG-MAL hydrogel with pediatric human bone cells regenerates critically sized craniofacial bone defects. *eLife*, **13**: RP92925.

Kang J, Chen JZ, Dong ZM, et al. 2021. The negative effect of the PI3K inhibitor 3-methyladenine on planarian regeneration via the autophagy signalling pathway. *Ecotoxicology*, **30**(9): 1941–1948.

Karki R, Malireddi RKS, Zhu QF, et al. 2017. NLRC3 regulates cellular proliferation and apoptosis to attenuate the development of colorectal cancer. *Cell Cycle*, **16**(13): 1243–1251.

Karki R, Man SM, Malireddi RKS, et al. 2016. NLRC3 is an inhibitory sensor of PI3K-mTOR pathways in cancer. *Nature*, **540**(7634): 583–587.

Lee KM, Park KH, Hwang JS, et al. 2018. Inhibition of STAT5A promotes osteogenesis by DLX5 regulation. *Cell Death & Disease*, **9**(11): 1136.

Li PH, Huang D. 2024. Targeting the JAK-STAT pathway in colorectal cancer: mechanisms, clinical implications, and therapeutic potential. *Frontiers in Cell and Developmental Biology*, **12**: 1507621.

Li YQ, Xu MK, Li YS, et al. 2021. Induction of $CD4^+$ regulatory T cells by stimulation with Staphylococcal Enterotoxin C2 through different signaling pathways. *Biomedicine & Pharmacotherapy*, **143**: 112204.

Lin JX, Ge ML, Liu CY, et al. 2024. Tyrosine phosphorylation of both STAT5A and STAT5B is necessary for maximal IL-2 signaling and T cell proliferation. *Nature Communications*, **15**(1): 7372.

Lin JX, Leonard WJ. 2000. The role of Stat5a and Stat5b in signaling by IL-2 family cytokines. *Oncogene*, **19**(21): 2566–2576.

Lv Y, Qi JX, Babon JJ, et al. 2024. The JAK-STAT pathway: from structural biology to cytokine engineering. *Signal Transduction and Targeted Therapy*, **9**(1): 221.

Müller J, Sperl B, Reindl W, et al. 2008. Discovery of chromone-based inhibitors of the transcription factor STAT5. *ChemBioChem*, **9**(5): 723–727.

Mustafa M, Ahmad R, Tantry IQ, et al. 2024. Apoptosis: a comprehensive overview of signaling pathways, morphological changes, and physiological significance and therapeutic implications. *Cells*, **13**(22): 1838.

O'Shea JJ, Schwartz DM, Villarino AV, et al. 2015. The JAK-STAT pathway: impact on human disease and therapeutic intervention. *Annual Review of Medicine*, **66**: 311–328.

Pan XY, Zeng YY, Liu YM, et al. 2023. Resolving vertebrate brain evolution through salamander brain development and regeneration. *Zoological Research*, **44**(1): 219–222.

Park C, Owusu-Boaitey KE, Valdes GM, et al. 2023. Fate specification is spatially intermingled across planarian stem cells. *Nature Communications*, **14**(1): 7422.

Pearson BJ, Eisenhoffer GT, Gurley KA, et al. 2009. Formaldehyde-based whole-mount in situ hybridization method for planarians. *Developmental Dynamics*, **238**(2): 443–450.

Peiris TH, Ramirez D, Barghouth PG, et al. 2016. The Akt signaling pathway is required for tissue maintenance and regeneration in planarians. *BMC Developmental Biology*, **16**(1): 7.

Peiris TH, Weckerle F, Ozamoto E, et al. 2012. TOR signaling regulates planarian stem cells and controls localized and organismal growth. *Journal of Cell Science*, **125**(Pt 7): 1657–1665.

Pellettieri J, Fitzgerald P, Watanabe S, et al. 2010. Cell death and tissue remodeling in planarian regeneration. *Developmental Biology*, **338**(1): 76–85.

Philips RL, Wang YX, Cheon H, et al. 2022. The JAK-STAT pathway at 30: much learned, much more to do. *Cell*, **185**(21): 3857–3876.

Qin Y, Wu K, Zhang Z, et al. 2022. NLRC3 deficiency promotes cutaneous wound healing due to the inhibition of p53 signaling. *Biochimica et Biophysica Acta (BBA) - Molecular Basis of Disease*, **1868**(11): 166518.

Reddien PW. 2018. The cellular and molecular basis for planarian regeneration. *Cell*, **175**(2): 327–345.

Reddien PW. 2021. Principles of regeneration revealed by the planarian eye. *Current Opinion in Cell Biology*, **73**: 19–25.

Shen BG, Wen Y, Lu SJ, et al. 2025. From injury to recovery: spatiotemporal dynamics of the visual pathway during spontaneous structural and functional regeneration after optic nerve transection in zebrafish. *Zoological Research*, **46**(4): 733–749.

Sun YJ, Ding N, Li SQ, et al. 2025. *NR1I3* modulates Wnt signaling to promote anterior-posterior axis patterning. *BMC Biology*, **23**(1): 231.

Surbek M, Tse W, Moriggl R, et al. 2021. A centric view of JAK/STAT5 in intestinal homeostasis, infection, and inflammation. *Cytokine*, **139**: 155392.

Verghese S, Su TT. 2016. *Drosophila* Wnt and STAT define apoptosis-resistant epithelial cells for tissue regeneration after irradiation. *PLoS Biology*, **14**(9): e1002536.

Wang QH, Sun XX, Xiao J, et al. 2022. *Djptpn11* is indispensable for planarian regeneration by affecting early wound response genes expression and the Wnt pathway. *Biochimie*, **201**: 184–195.

Wenemoser D, Reddien PW. 2010. Planarian regeneration involves distinct stem cell responses to wounds and tissue absence. *Developmental Biology*, **344**(2): 979–991.

Williams MJ, Wang XN, Bastos HP, et al. 2025. Maintenance of hematopoietic stem cells by tyrosine-unphosphorylated STAT5 and JAK inhibition. *Blood Advances*, **9**(2): 291–309.

Wurtzel O, Cote LE, Poirier A, et al. 2015. A generic and cell-type-specific wound response precedes regeneration in planarians. *Developmental Cell*, **35**(5): 632–645.

Xie JM, Chen YR, Cai GJ, et al. 2023. Tree Visualization By One Table (tvBOT): a web application for visualizing, modifying and annotating phylogenetic trees. *Nucleic Acids Research*, **51**(W1): W587–W592.

Xin P, Xu XY, Deng CJ, et al. 2020. The role of JAK/STAT signaling pathway and its inhibitors in diseases. *International Immunopharmacology*, **80**: 106210.

Xue C, Yao QF, Gu XY, et al. 2023. Evolving cognition of the JAK-STAT signaling pathway: autoimmune disorders and cancer. *Signal Transduction and Targeted Therapy*, **8**(1): 204.

Zeng A, Li H, Guo LH, et al. 2018. Prospectively isolated $Tetraspanin^+$ neoblasts are adult pluripotent stem cells underlying planaria regeneration. *Cell*, **173**(7): 1593–1608. e20.

Zeng A, Li YQ, Wang C, et al. 2013. Heterochromatin protein 1 promotes self-renewal and triggers regenerative proliferation in adult stem cells. *Journal of Cell Biology*, **201**(3): 409–425.

Zhen H, Huang MJ, Zheng MY, et al. 2023. WTAP regulates stem cells via TRAF6 to maintain planarian homeostasis and regeneration. *International Journal of Biological Macromolecules*, **242**(Pt 3): 124932.

Zheng HX, Li LF, Wang D, et al. 2025. FoxO is required for neoblast differentiation during planarian regeneration. *International Journal of Biological Macromolecules*, **288**: 138729.

Zheng HX, Liu HB, Xu Q, et al. 2021. PI3K plays an essential role in planarian regeneration and tissue maintenance. *Frontiers in Cell and Developmental Biology*, **9**: 649656.